*clean technologies*

MDPI

*Article*

# Rate-Based Modeling and Sensitivity Analysis of Potassium Carbonate Systems for Carbon Dioxide Capture from Industrial Flue Gases

**Giannis Pachakis [1,*], Sofia Mai [1,*], Elli Maria Barampouti [1] and Dimitris Malamis [2]**

[1] Unit of Environmental Science and Technology, School of Chemical Engineering, National Technical University of Athens, 9 Iroon Polytechniou, Zografos, 15772 Athens, Greece; belli@central.ntua.gr
[2] Department of Civil and Environmental Engineering, College of Engineering, Design & Physical Sciences, Brunel University of London, London UB8 3PH, UK; dimitris.malamis@brunel.ac.uk
* Correspondence: gpachakis@mail.ntua.gr (G.P.); mai@central.ntua.gr (S.M.)

**Abstract**

The increasing atmospheric concentration of carbon dioxide ($CO_2$) poses a critical threat to global climate stability, highlighting the need for efficient carbon capture technologies. While amine-based solvents such as monoethanolamine (MEA) are widely used for industrial $CO_2$ capture, they are subject to limitations such as high energy requirements for regeneration, solvent degradation, and environmental concerns. This study investigates potassium carbonate/bicarbonate system as an alternative solution for $CO_2$ absorption. The absorption mechanism and reaction kinetics of potassium carbonate in the presence of bicarbonates were reviewed. A rate-based model was developed in Aspen Plus, using literature kinetics, to simulate $CO_2$ absorption using 20 wt% potassium carbonate ($K_2CO_3$) solution with 10% carbonate-to-bicarbonate conversion under different industrial conditions. Three flue gas compositions were evaluated: cement industry, biomass combustion, and anaerobic digestion, each at 3000 $m^3$/h flow rate. The simulation was conducted to determine minimum column height and solvent loading requirements with a target output of 90% $CO_2$ removal from the gas streams. Results demonstrated that potassium carbonate systems successfully achieved the target removal efficiency across all scenarios. Column heights ranged from 18 to 25 m, with molar $K_2CO_3/CO_2$ ratios between 1.41 and 4.00. The biomass combustion scenario proved most favorable due to lower $CO_2$ concentration and effective heat integration. While requiring higher column heights (18–25 m) compared to MEA systems (6–12 m) and greater solvent mass flow rates, potassium carbonate demonstrated technical feasibility for $CO_2$ capture. The findings of this study provide a foundation for technoeconomic evaluation of potassium carbonate systems versus amine-based technologies for industrial carbon capture applications.

**Keywords:** carbon capture; chemical absorption; potassium carbonate; Aspen Plus; simulation; sensitivity analysis



Academic Editor: Xianfeng Fan

Received: 12 November 2025
Revised: 16 December 2025
Accepted: 6 January 2026
Published: 19 January 2026



## 1. Introduction

The concentration of carbon dioxide ($CO_2$) in earth's atmosphere has increased from 278 ppm in 1750 [1] to 425.2 ± 0.1 ppm in 2024 [2]. Over the course of these years, emerging technologies and heavy industrialization have seen remarkable growth. The intensified human activities have significantly contributed to greenhouse gas emissions and mainly to carbon dioxide. This trend poses a serious threat to the environment by undermining

climate stability, ecosystem resilience, and long-term sustainability. In the last 60 years alone, atmospheric $CO_2$ concentration has increased by approximately 105 ppm with an increasing rate of accumulation as shown in Figure 1.

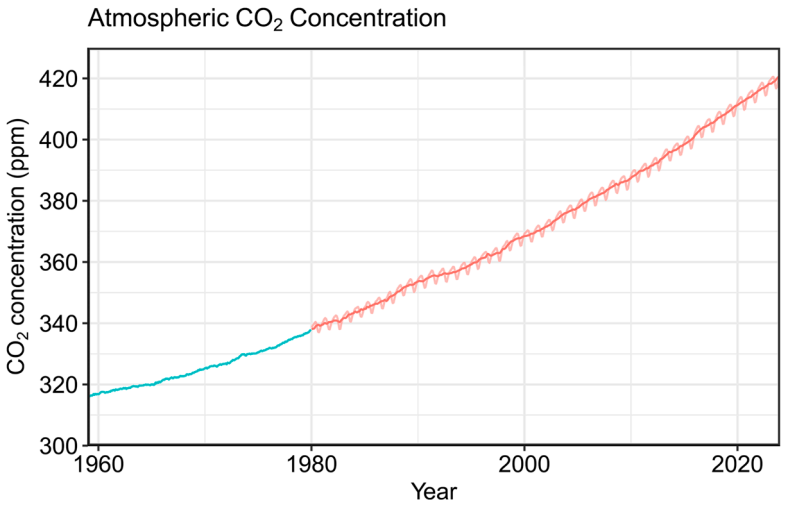


**Figure 1.** Surface atmospheric $CO_2$ concentration. Adapted from [3].

Industry sectors such as cement, steel and power are among the largest contributors, with the cement industry alone responsible for approximately 7–8% of global anthropogenic $CO_2$ emissions due to both fossil fuel combustion and the calcination of limestone during clinker production [4]. In addition to fossil fuel combustion, biomass burning also contributes greatly to these emissions. In 2023 biomass burning was responsible for 2% of global $CO_2$ emissions [5].

The need to reverse the increasing trend in greenhouse gas emissions has led to international climate targets such as those delineated in the Paris Agreement [6]. To meet these targets, large-scale reduction in $CO_2$ is essential as reported in [7]. Among available strategies, carbon capture and storage (CCS) and carbon capture and utilization (CCU) seem to play key roles for decarbonization. While geological sequestration of $CO_2$ gains attention, utilization pathways offer a more circular and economically attractive solution, by using $CO_2$ as a raw material for the production of fuels, chemicals, or biologically derived products [8].

Particularly, biofixation serves as a promising route of valorization, wherein captured $CO_2$ is supplied to microalgae as carbon source to enhance biomass production that can be further processed to biofuels, biomaterials, or animal feed [9,10]. Other routes include thermochemical conversion into methanol [11], urea [12], mineralization [13], and synthetic fuels [14]. In any of these cases, the applicability, scalability and cost-effectiveness of these downstream processes are critically related to the quality and scalability of the upstream capture process.

Chemical absorption is among the most mature and widely implemented technologies, especially for post-combustion $CO_2$ removal [15]. Amine-based solvents are the most used chemical species by the industry of chemical absorption. Specifically, monoethanolamine (MEA) is the dominant solvent in commercial applications due to its high reactivity and reaction kinetics with $CO_2$ [16].

However, MEA and amine-based systems face several drawbacks and limitations to their use. Its main drawback is the high heat of reaction with $CO_2$ (85.6 kJ/mol$_{CO2}$) [17]. This leads to increased energy requirements for stripping. Notably, the energy demand is reported to be between 3.9 and 4.2 GJ/ton$_{CO2}$ [18].

Solvent degradation is a critical issue, as it is related to the formation of unwanted by-products and increased operating costs. Carbamate polymerization is the most common degradation mechanism for amines in the presence of $CO_2$ and elevated temperatures [19]. The rate of polymerization is strongly dependent on $CO_2$ concentration [20], thus hindering the solvent's regeneration efficiency when treating gas streams with higher concentration in $CO_2$. Another common mechanism is oxidative degradation which occurs by the unwanted reaction of the solvent into various chemicals in the presence of oxygen which is found in higher concentrations in post-combustion flue gas due to the excess of air. The oxidative degradation of amine-based solvents leads to the formation of a range of by-products, including aldehydes, low-molecular-weight organic acids (e.g., acetate, formate, and glycolate), amine salts such as oxalates, as well as ammonia and nitrosamine compounds [21]. Monoethanolamine is also reported to have a corrosive behavior [22] and high impact on fresh water ecotoxicity [23].

As a result of these limitations, alternative solvents are actively being investigated [24]. Recent "second-generation" solvent development has focused on hindered/tertiary amines and blends with Piperazine (e.g., MDEA/PZ and other promoted amines) to lower regeneration energy and improve cyclic capacity relative to conventional MEA systems. Nevertheless, the broader amine-solvent family, still faces practical drawbacks linked to solvent degradation (oxidative/thermal), corrosion, solvent loss, and formation of potentially harmful degradation products (e.g., nitrosamines/nitramines) in systems exposed to $O_2/NO_x$ and elevated temperatures, all of which can translate into operational complexity and added cost for solvent management and emissions control [25].

A recent study on advanced amine and phase-change solvents, including conventional MEA, blended with Dimethylethanolamine and Triethylene glycol monomethyl ether forming systems such as DMEA/MAE, and biphasic formulations based on DMEA/MAE/TGME, show that gains in regeneration energy efficiency are often accompanied by practical limitations. Although blended and biphasic solvents can enhance cyclic capacity and reduce calculated regeneration duties compared to MEA, reported results consistently point to challenges associated with the high viscosity of the $CO_2$-rich phase, which can hinder mass transfer, narrow the operating window of packed columns, and increase pumping demands. Phase-change solvents also introduce additional constraints, including the need for careful control of the phase-change loading to avoid premature separation within the absorber, as well as possible losses in overall energy efficiency associated with the enthalpy of phase separation. Moreover, the literature points to a clear trade-off between minimizing energy consumption and achieving adequate $CO_2$ removal efficiency under industrially relevant operating conditions. Overall, these findings suggest that, despite their promising thermodynamic characteristics, advanced amine and biphasic solvent systems remain limited by issues related to viscosity, phase behavior, and process operability [26]. Against this landscape, potassium carbonate ($K_2CO_3$), poses a promising option as it is characterized by low volatility, chemical stability under typical operating conditions, relatively low cost and minimal environmental impacts. The post absorption solution, rich in potassium, carbonates and bicarbonates, has also shown potential as a biofertilizer for algae cultivation ponds and bioreactors [27], promoting circular economy and sustainability principles.

Potassium-rich, bicarbonate-based solutions derived from $CO_2$ capture processes are compatible with typical microalgae cultivation systems, including open raceway ponds and closed photobioreactors, where dissolved inorganic carbon is commonly supplied in bicarbonate form rather than exclusively as gaseous $CO_2$. Multiple studies have shown that microalgae such as *Chlorella* and *Spirulina* can tolerate and assimilate elevated concentrations of bicarbonate in aqueous media, with growth sustained across a broad range of ionic

strengths depending on species, pH control, and cultivation configuration. In particular, bicarbonate-based carbon delivery has been demonstrated under controlled photobioreactor conditions as well as in hybrid capture–cultivation systems relevant to pond operation, indicating that moderate potassium and alkalinity levels typical of alkaline growth media do not inherently limit algal productivity. These observations support the feasibility of coupling potassium-rich $CO_2$ capture solutions with algae cultivation, provided that ionic strength and alkalinity are managed within species-specific tolerance ranges reported in the algae cultivation literature [28–30].

Nevertheless, potassium carbonate systems face a specific drawback. The $K_2CO_3$-$CO_2$ system is inherently slower than amine-based or strong electrolyte systems. This can be overcome by adjusting other operational factors such as temperature, packed section height, and molar liquid-to-gas (L/G) ratio [31].

Despite the extensive body of simulation work on carbon capture, MEA and amine-based systems [32–37], there are relatively few to no studies that have examined how process parameters such as temperature, L/G ratio, and column height affect $CO_2$ removal yield in potassium carbonate-based systems. This study aims to address the existing gaps by designing and modeling a $CO_2$ absorber using $K_2CO_3$-$KHCO_3$ in Aspen Plus. The effects of these process parameters will be assessed.

The primary objective is to evaluate the technical feasibility of achieving over 90% $CO_2$ removal yield with potassium carbonate solvent and to identify the key design parameters necessary for effective performance across various flue gas compositions. Specifically, three different emission profiles are considered: cement production, biomass combustion and biogas derived from anaerobic digestion. The absorber is designed for a gas flow rate of 3000 $m^3$/h, which is approximately the biogas production of a 5 MW anaerobic digestion unit which is considered a representative and realistic scale for both industrial and regional organic waste management. It is a size that can be economically viable while still addressing significant waste streams, making it a practical option for various applications [38,39].

This capacity is applied across all scenarios, so the results are comparable between the different gas compositions. The findings of this work aim to provide the carbon capture industry with crucial insights into the use of potassium carbonate as a solvent and to inform the development of energy-efficient absorption configurations that can facilitate a more sustainable and circular approach to the $CO_2$ management strategies.

## 2. Materials and Methods

### *2.1. Process Chemistry*

The physical and chemical mechanisms occurring during the absorption of $CO_2$ are well explained in [40,41]. The reactions occurring during the process can be described with the following equations:

$$CO_{2(g)} \rightleftharpoons CO_{2(aq)} \quad (1)$$

$$CO_{2(aq)} + H_2O \rightarrow HCO_3^- + H^+ \quad (2)$$

$$CO_{2(aq)} + OH^- \rightarrow HCO_3^- \quad (3)$$

$$HCO_3^- \rightarrow CO_{2(aq)} + OH^- \quad (4)$$

$$H_2O \rightleftharpoons OH^- + H^+ \quad (5)$$

Equation (1) represents the physical phase equilibrium of $CO_2$ at the interface of the gas and the liquid. The equilibrium of Equation (1) is governed by Henry's law:

$$C_i = HP_i \quad (6)$$

where $C_i$ is the concentration of the aqueous gas on the liquid phase, $H$ is Henry's constant and $P_i$ is partial pressure of the gas in the gas phase [42].

In the well-known work of [43–46], it is suggested that the kinetic factor of Equation (3) is depended on the ionic strength of the solvent as described below:

$$\log k_{OH} = \log k_{\infty} + bI \tag{7}$$

where $k_{\infty}$ is rate constant in infinite dilution, $b$ is a temperature dependent coefficient, and $I$ is the ionic strength of the solution. This kinetic expression has been tested and validated in [47]. Although the reaction kinetics in the previously described work have been thoroughly studied, they are not applicable for weak electrolytes such as carbonic salts. When carbonate and bicarbonate ions are present, the following reaction takes place and plays a significant role in the overall kinetic mechanism.

$$CO_3^{2-} + H_2O \rightleftharpoons HCO_3^- + OH^- \tag{8}$$

In [48] it is stated that the overall reaction rate of the $CO_2$ can be expressed as

$$r_{abs} = -\frac{d[CO_2]}{dt} = k_{ov}[CO_2] \tag{9}$$

where $r$ (kmol m$^{-3}$ s$^{-1}$) is the rate of the absorption $CO_2$, [$CO_2$] (kmol m$^{-3}$) is the concentration of aqueous species of $CO_2$ in the liquid, $t$ is the time and $k_{ov}$ (s$^{-1}$) is the overall constant for the first order rate given by the following equation:

$$k_{ov} = k_{H_2O} + k_{OH}[OH^-] \tag{10}$$

where $k_{H_2O}$ (s$^{-1}$) is the first order constant for reaction (2) and $k_{OH}$ (m$^3$ kmol$^{-1}$ s$^{-1}$) the second order constant for Equation (3). The $k_{H_2O}$ factor is significantly smaller than $k_{OH}$, hence it is considered negligible [49]. The equilibrium of Equation (8) is instantaneous [27]. The concentration of $OH^-$ ions in the solution is driven by the ionic equilibrium equation:

$$K_b = \frac{[OH^-][HCO_3^-]}{[CO_3^{2-}]} \tag{11}$$

where $K_b$ is the equilibrium constant of Equation (8). During the absorption process with dilute solutions, the relative change in $[HCO_3^-]$ and $[CO_3^{2-}]$ is small, thus the $[OH^-]$ remains almost constant. Overall, the final absorption rate as described in Equation (9) is regarded as a pseudo-first-order reaction with respect to $CO_2$ [43,45,46].

### *2.2. Process Modelling*

#### 2.2.1. Components and Methods

The simulation model was developed in Aspen Plus V12. The ELECNRTL (Electrolyte Non-Random Two Liquid) method was used for the calculation of the liquid phase properties, while the RK (Redlich-Kwong) equation of state was used to retrieve properties of the vapor phase. ELECNRTL was selected as the most versatile and accurate model for both low and high concentrations of aqueous mixed solvent systems. The following components represent the chemical species in the process as shown in Table 1.

**Table 1.** Chemical components of the simulation in Aspen Plus.

| Component ID | Type | Component Name | Alias |
|---|---|---|---|
| H2O | Conventional | WATER | H2O |
| CO2 | Conventional | CARBON-DIOXIDE | CO2 |
| N2 | Conventional | NITROGEN | N2 |
| O2 | Conventional | OXYGEN | O2 |
| CH4 | Conventional | METHANE | CH4 |
| K2CO3 | Conventional | POTASSIUM-CARBONATE | K2CO3 |
| KHCO3 | Conventional | POTASSIUM-BICARBONATE | KHCO3 |
| HCO3− | Conventional | HCO3− | HCO3− |
| CO3−2 | Conventional | CO3−− | CO3−2 |
| K+ | Conventional | K+ | K+ |
| H3O+ | Conventional | H3O+ | H3O+ |
| OH− | Conventional | OH− | OH− |

Components $CO_2$, $N_2$, $O_2$, $CH_4$ are selected as Henry-components and their temperature dependent binary parameters with $H_2O$ are retrieved from the Aspen Plus databanks. The $CO_2$ parameters were retrieved from APV110 ENRTL-RK, while the parameters of the remaining components were retrieved from APV110 BINARY. The fitted temperature validity ranges span approximately 0–227 °C for $CO_2$–$H_2O$, 0–73 °C for $N_2$–$H_2O$, 1–75 °C for $O_2$–$H_2O$, and 1–72 °C for $CH_4$–$H_2O$. These ranges encompass the operating temperatures encountered in the absorber unit considered in this study. The parameters are pressure-independent within the moderate pressure range investigated, consistent with their use in vapor–liquid equilibrium and activity-coefficient calculations for low- to medium-pressure gas absorption systems.

#### 2.2.2. Flue Gas Cases

The carbon capture model is developed for flue gases from: the cement industry, biomass combustion and anaerobic digestion. The volumetric flow rate is set at 3000 $m^3/h$ for each case. The conditions and compositions of the flue gas stream are given in Table 2, which were retrieved from literature.

**Table 2.** Flue gas parameters and composition.

| Parameter | Cement Plant [50] | Biomass Combustion [51] | Anaerobic Digestion Plant [52] |
|---|---|---|---|
| Mass rate (kg/h) | 3344.9 | 2972.7 | 3718.7 |
| Temperature (°C) | 130 | 130 | 35 |
| Pressure (bar) | 1.2 | 1.2 | 1.2 |
| *Mol fractions* | | | |
| $H_2O$ | 0.11 | 0.2 | 0.05 |
| $CO_2$ | 0.22 | 0.06 | 0.35 |
| $N_2$ | 0.6 | 0.66 | - |
| $O_2$ | 0.07 | 0.08 | - |
| $CH_4$ | - | - | 0.6 |

To place the three case studies in a broader industrial context, the selected flue gas compositions were benchmarked against typical operating ranges reported for full-scale plants. Coal-fired utility boilers generally exhibit stack gas $CO_2$ concentrations of 7–15 mol%, whereas natural-gas-fired power plants are typically in the range of 3–4 mol% $CO_2$ [53]. Biomass combustion in industrial boilers and fluidized-bed units produces similar or slightly lower $CO_2$ levels (approximately 5–10 vol%), depending on excess air and fuel moisture content [53,54]. The biomass combustion case adopted in this work (6 mol% $CO_2$,

20 mol% $H_2O$) therefore lies well within the range measured for operating biomass plants and is consistent with literature data for wood-chip combustion units.

For cement production, modern dry-process kilns typically generate flue gases with $CO_2$ concentrations between about 15 and 25 mol%, depending on raw meal composition, degree of calcination and fuel mix [55]. Schakel et al. report a representative cement-plant stack gas with 17.8 mol% $CO_2$ and 18.2 mol% $H_2O$ [56], while lab-scale capture tests have used synthetic cement flue gas streams containing 20 vol% $CO_2$. The cement case considered here (22 mol% $CO_2$, 11 mol% $H_2O$) is thus representative of real kiln conditions and reflects the fact that the cement industry is responsible for approximately 7–8% of global anthropogenic $CO_2$ emissions.

Anaerobic digestion plants typically produce raw biogas streams containing around 35–45 vol% $CO_2$ and 55–65 vol% $CH_4$ at near-ambient temperature, depending on substrate and operating conditions [57]. The anaerobic digestion case in this study (35 mol% $CO_2$, 60 mol% $CH_4$, 5 mol% $H_2O$) closely matches these reported compositions and can be regarded as representative of biogas upgrading applications. Taken together, the three flue gas cases therefore span a realistic range of low-, medium- and high-$CO_2$ streams encountered in large stationary sources (biomass boilers, cement kilns and biogas plants), which are among the primary targets for post-combustion $CO_2$ capture and utilization technologies [58].

#### 2.2.3. Process Flowsheets

A rate-based model is used to develop the process flowsheets of Figures 2 and 3. The absorber is considered the main process. RadFrac module is selected as the most rigorous model for simulating all types of multistage vapor-liquid fractionation operations. The heat exchanger (EX-1) is set to return a hot stream outlet temperature of 50 °C. As a result, the liquid solvent temperature reduces as the L/G ratio is increasing. The dehumidifier (COND-1) is a flash column with zero duty and zero pressure drop to trap and remove the water vapor condensates that hinder the $CO_2$ removal efficiency. In Table 3 the model and design parameters are presented for the absorbing column.

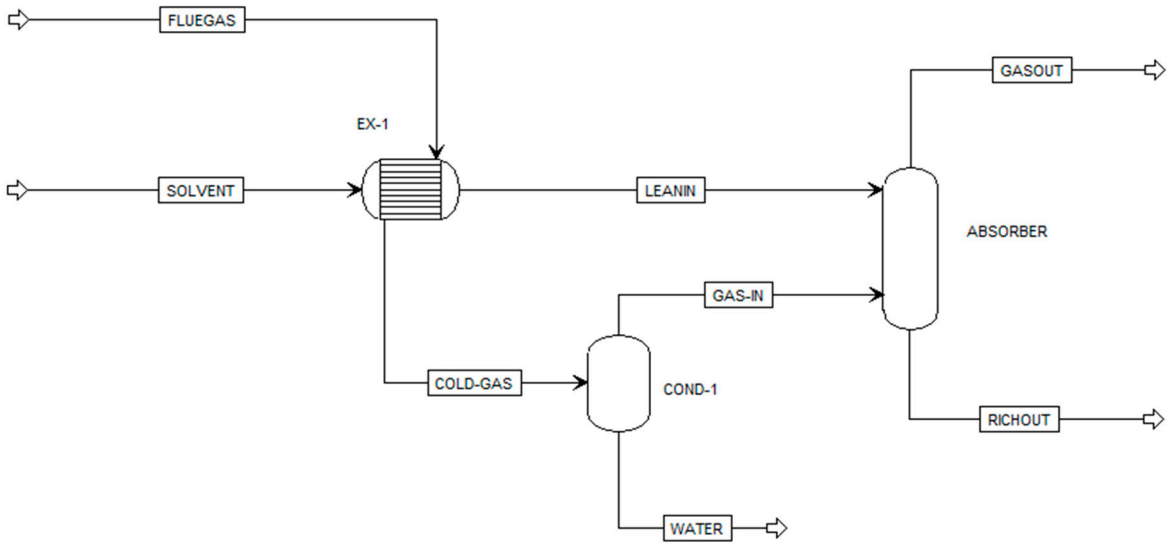


**Figure 2.** Process flowsheet of gas absorption for cement and biomass combustion units.

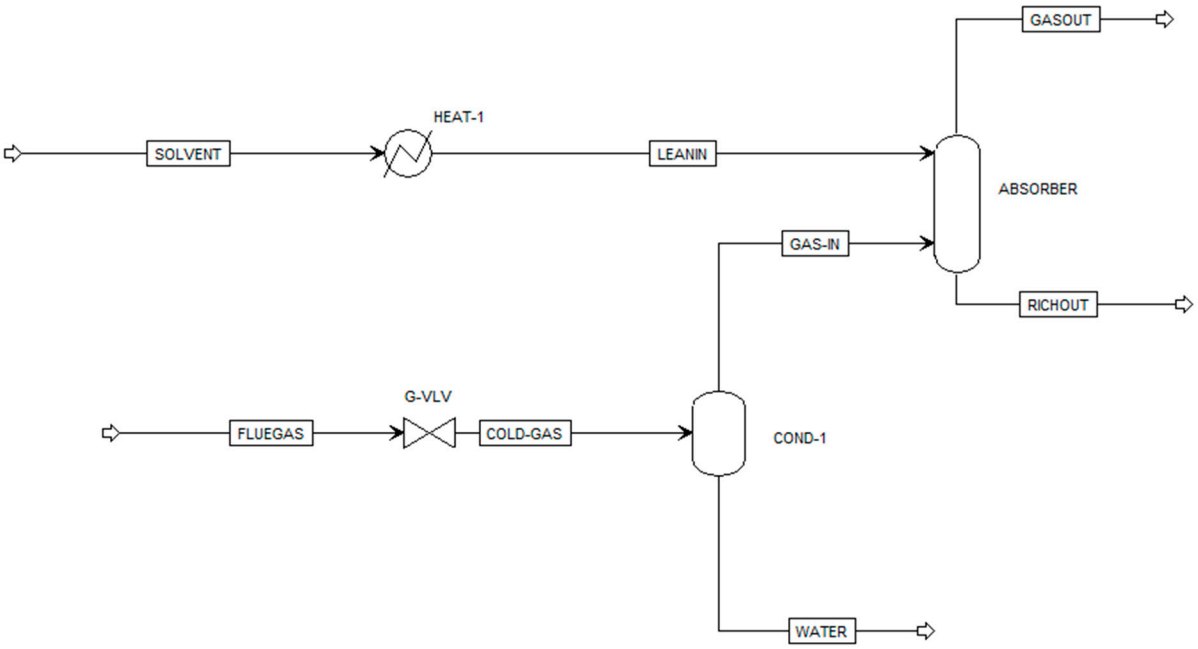


**Figure 3.** Process flowsheet of gas absorption for the anaerobic digestion unit.

**Table 3.** Aspen Plus model and design specifications for the RadFrac column.

| Specification | Parameter Value |
|---|---|
| Number of stages | 18 |
| Operating pressure | 1 bar |
| Re-boiler | None |
| Condenser | None |
| Packing type | Berl saddles, ceramic, 13 mm |
| Packing height range | 18–25 m |
| Packing diameter | 1.2 m (1.6 m for AD unit) |
| Reaction condition factor | 0.9 * |
| Mass transfer coefficient | Onda68 [59] |
| Interfacial area method | Onda68 [59] |
| Interfacial area factor | 2 |
| Heat transfer coefficient method | Chilton and Colburn |
| Holdup correlation | Stichlmair89 [60] |
| Liquid film resistance | Discretization, 5 points |
| Vapor film resistance | Film consideration |
| Flow model | Mixed |

* A reaction condition factor of 0.9 was applied in the RadFrac model to account for non-ideal reactive mass transfer and to avoid assuming ideal equilibrium conditions on each theoretical stage.

The absorber column diameter was determined based on hydraulic constraints to ensure operation within a target flooding range of 45–75%. Flooding velocity was estimated using the packed-column hydraulic models implemented in Aspen Plus (RadFrac), accounting for the specified gas and liquid mass flow rates, fluid properties, and packing characteristics. In the Anaerobic Digestion configuration, the higher total mass flow rate led to increased superficial gas velocity and liquid loading, resulting in predicted flooding fractions above the acceptable range when a column diameter of 1.2 m was applied. The column diameter was therefore increased to 1.6 m to reduce superficial velocities and maintain operation within the prescribed flooding window. This adjustment ensured hydraulically feasible operation while keeping the absorber design consistent with the comparative scope of the study. The packing material used in the simulation was 13 mm ceramic Berl saddles. Ceramic packing was selected due to its compatibility with aqueous

potassium carbonate/bicarbonate systems, which operate under alkaline conditions and can impose corrosion constraints on metallic materials. Inert ceramic packings are commonly reported for potassium carbonate absorption processes due to their resistance to chemical degradation and suitability for operation over the temperature range relevant to absorption and regeneration. The nominal size of 13 mm was chosen to provide a balance between effective interfacial area and hydraulic capacity, allowing operation within the targeted flooding range for the investigated gas and liquid flow rates [27].

The biogas produced by the anaerobic unit is usually at 35 °C and so the heat integration cannot be applied at this scenario. This excludes the use of the heat exchanger between the gas stream and the liquid solvent. A heat exchanger is introduced only for the liquid stream and is set to return a cold stream outlet temperature of 45 °C as presented in Figure 3.

#### 2.2.4. Reaction Kinetics

In the work of Ye and Lu [48], an extensive assessment of the $CO_2$ absorption reaction kinetics in different $K_2CO_3$-$KHCO_3$ solutions was performed. Their results showed that higher concentrations of $K_2CO_3$ in the solvent promote the rate of the reaction, while an increase in carbonate-to-bicarbonate (CTB) conversion lowers the reaction's activation energy $E_\alpha$ making it more favorable in higher temperatures. They came down to four different equations that correlate the Arrhenius' preexponential factor with solution's ionic strength and CTB as presented below:

$$\ln(\mathrm{A}) = 0.24I + 26.40, \ (\alpha = 0\%) \quad (12)$$

$$\ln(\mathrm{A}) = 0.43I + 23.39, \ (\alpha = 10\%) \quad (13)$$

$$\ln(\mathrm{A}) = 0.50I + 19.79, \ (\alpha = 20\%) \quad (14)$$

$$\ln(\mathrm{A}) = 0.64I + 17.83, \ (\alpha = 40\%) \quad (15)$$

and to an equation for correlating $E_\alpha$ with CTB

$$E_\alpha = 171.10\alpha^2 - 128.74\alpha + 47.03 \quad (16)$$

Figures 4 and 5 present the behavior of the pre-exponential factor A and of the activation energy $E_\alpha$ for the different values of $\alpha$.

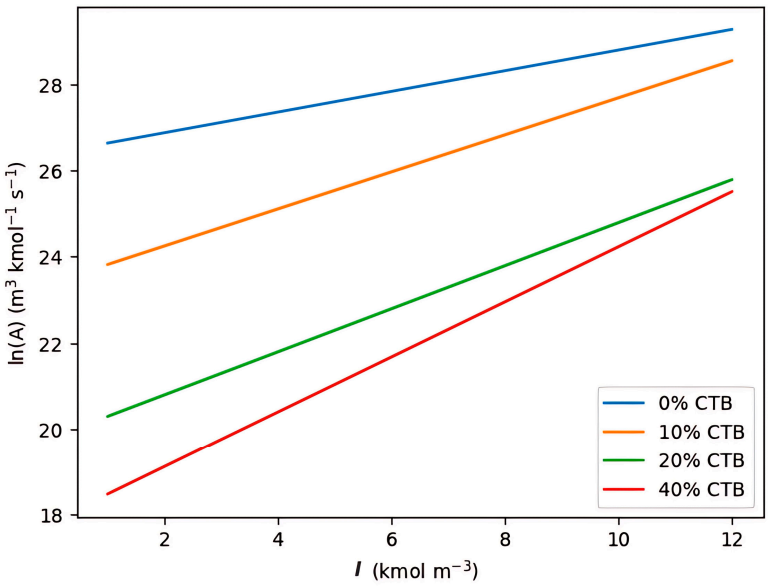


**Figure 4.** Variation in ln(A) with $I$ for different values of $\alpha$ (0–40%).

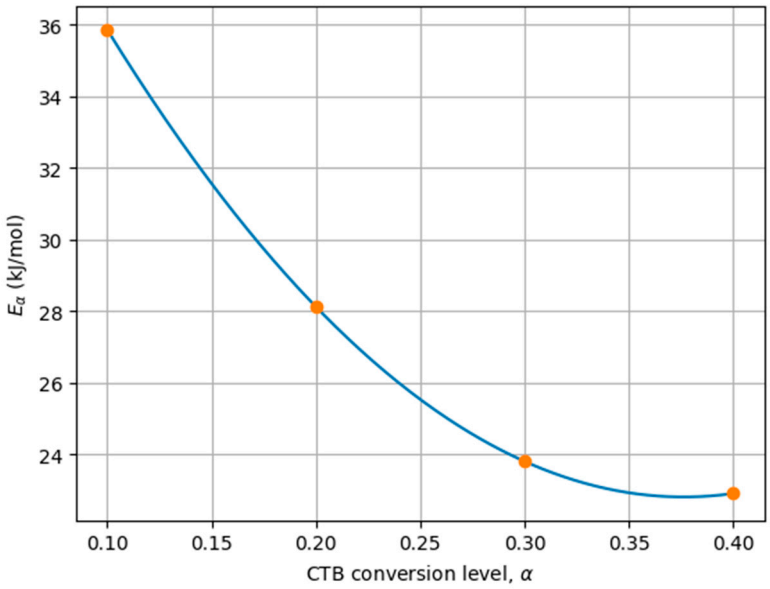


**Figure 5.** Correlation of the activation energy $E_\alpha$ with $\alpha$ based on the fitted quadratic relationship.

For this simulation model a solvent stream with 20 wt% in $K_2CO_3$ has been assessed with 10% CTB. The kinetics of Equations (3) and (4) are presented in Table 4.

**Table 4.** Reaction kinetics parameters.

| Parameter | Kinetic Factor | Activation Energy (kJ/mol) |
|---|---|---|
| Equation (3) | $1.1458 \times 10^{11}$ | 35.89 |
| Equation (4) | $2.83 \times 10^{17}$ | 123.3 |

For Equations (5) and (7) the equilibrium constants $K_j$ are calculated by the following equation:

$$\ln(K_j) = A_j + \frac{B_j}{T} + C_j \ln(T) + D_j T \quad (17)$$

The constants of Equation (17) are presented in Table 5.

**Table 5.** Equilibrium parameters.

| Parameter | $A_j$ | $B_j$ | $C_j$ | $D_j$ |
|---|---|---|---|---|
| Equation (5) | 132.899 | −13,445.9 | −22.4773 | 0 |
| Equation (8) | 216.049 | −12,431.7 | −35.4819 | 0 |

2.2.5. Sensitivity Analysis

A sensitivity analysis was performed for each scenario on the molar L/G ratio and on the column height to assess the $CO_2$ removal yield, which is the percentage of the removed $CO_2$ from the gas stream entering the column. The removal yield is promoted by both parameters. Initially, an L/G sensitivity analysis was carried out to define the effective operating range for each scenario. Subsequently, a parallel sensitivity analysis of the column height was introduced, and the optimal points could be identified. The target $CO_2$ removal was 90% of the inlet concentration. Two minimum points were identified for each case: one at minimum column height and one at minimum L/G ratio.

## 3. Results

### *3.1. Model Outputs*

Table 6 summarizes the major parameters of the solvent streams under each scenario, based on the respective solvent loading range.

**Table 6.** Solvent parameters and ranges for each case.

| Parameter | Cement Plant | Biomass Combustion | Anaerobic Digestion |
|---|---|---|---|
| mol $K_2CO_3$/mol $CO_2$ | 1.75–4.00 | 1.75–2.75 | 1.25–2.00 |
| Mass flow (kg/h) | 27,408.4–43,070.4 | 8155.8–12,816.2 | 44,743.2–71,589.1 |
| Solvent/Gas mass ratio | 8.19–12.88 | 2.74–4.31 | 12.03–19.25 |
| Column height (m) | 20–25 | 18–23 | 18–23 |
| Temperature (°C) | 24.5–23.2 | 47.8–41.6 | 45 |
| Concentration wt% | 20 | 20 | 20 |

The results of the initial sensitivity analyses are presented in Figures 4–6. As expected, the $CO_2$ removal yield increases with an increasing L/G ratio. Figure 6 demonstrates a weaker correlation between the L/G and the removal efficiency, whereas Figures 7 and 8 exhibit a greater relationship. Figure 7 shows that the $CO_2$ removal efficiency for biomass combustion flue gas increases with the L/G ratio up to a maximum, beyond which a decline is observed. This behavior can be interpreted in terms of enthalpy fluxes between the phases: at higher L/G ratios, the enthalpy flux carried by the colder liquid stream exceeds the latent enthalpy flux available from water vapor in the hot flue gas. As a result, the interfacial temperature decreases, reducing solvent capacity and the mass-transfer driving force for $CO_2$ absorption, and leading to a maximum in removal efficiency at the specific operating configuration.

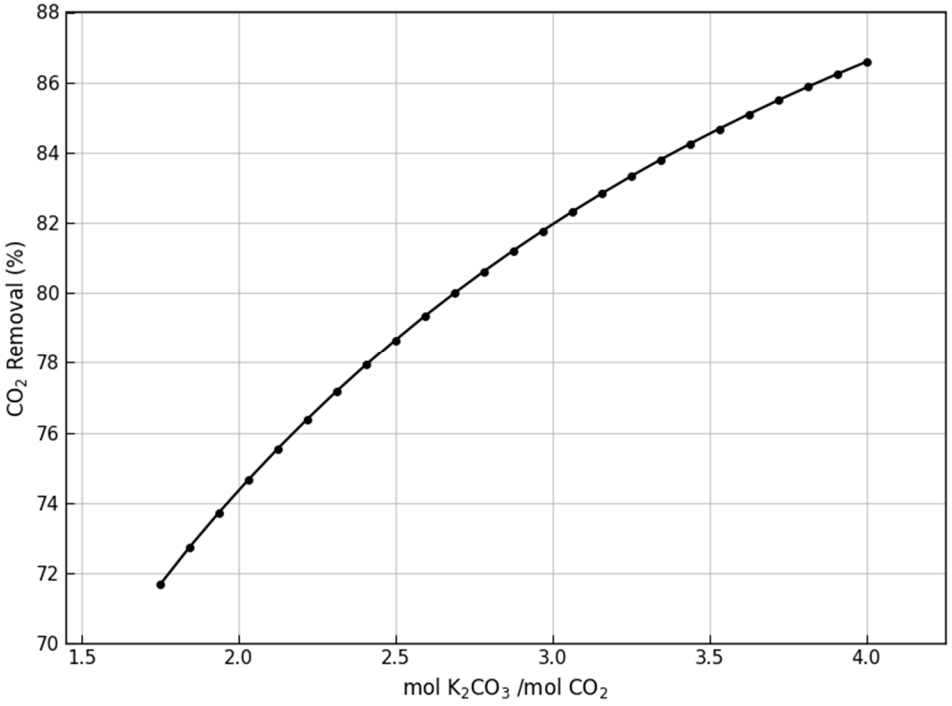


**Figure 6.** L/G ratio sensitivity analysis for the cement industry flue gas (column height = 20 m).

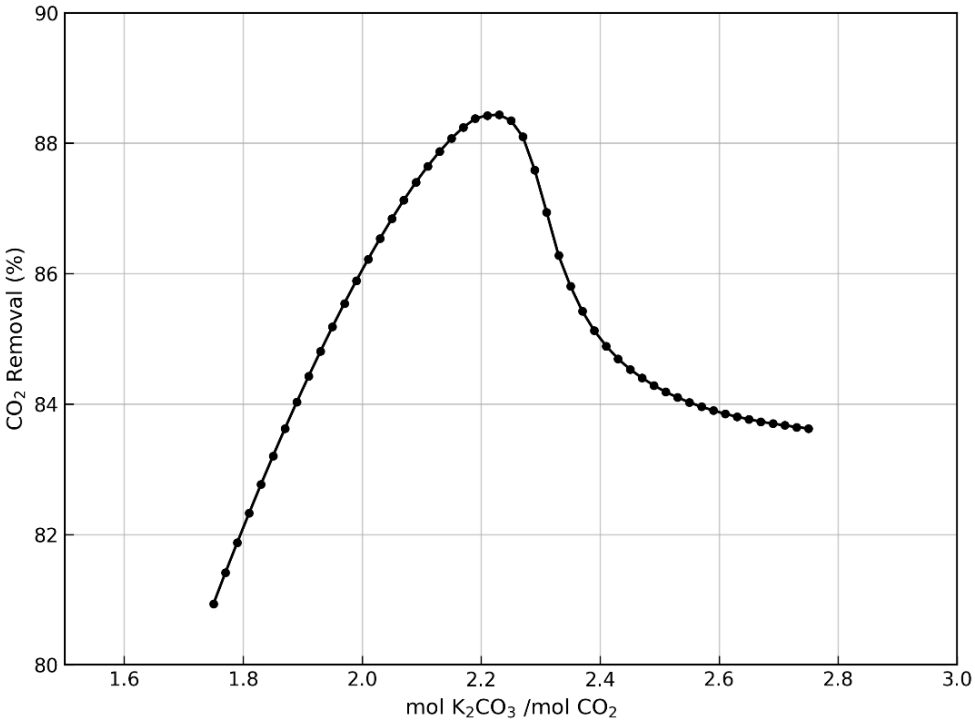


**Figure 7.** L/G ratio sensitivity analysis for the biomass combustion flue gas (column height = 18 m).

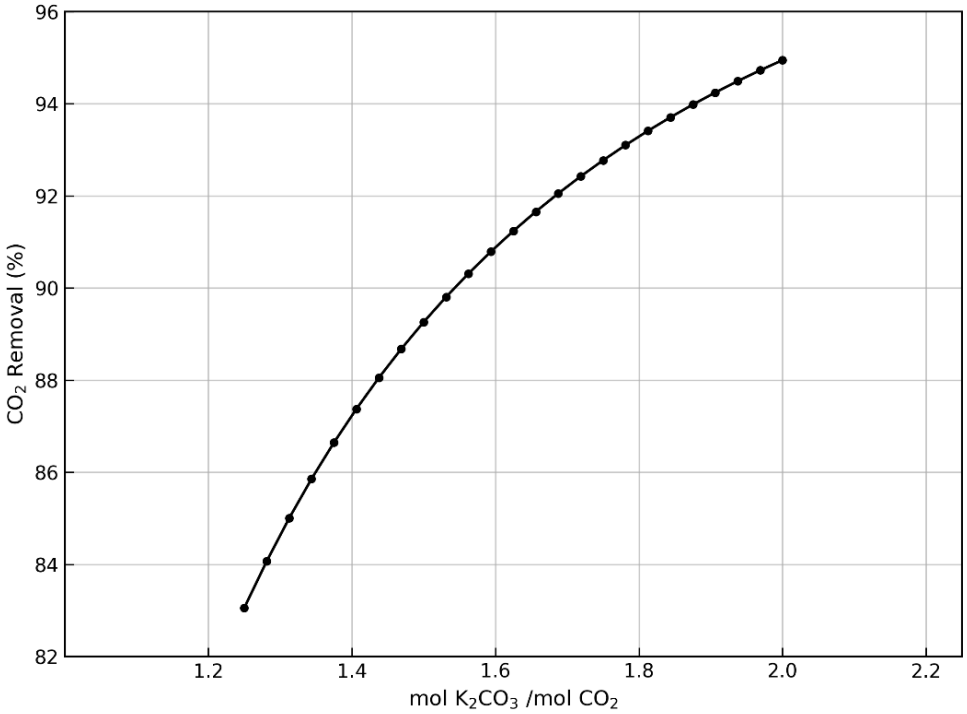


**Figure 8.** L/G ratio sensitivity analysis for the anaerobic digestion biogas (column height = 18 m).

Figures 9–11 present the 3D plot of $CO_2$ removal as a function of column height and solvent loading in terms of mol $K_2CO_3$ per mol of $CO_2$. As expected, increasing the column height promotes removal efficiency as a taller column provides more contact time for the mass transfer mechanism, while higher solvent loading promoted the chemical absorption's driving force.

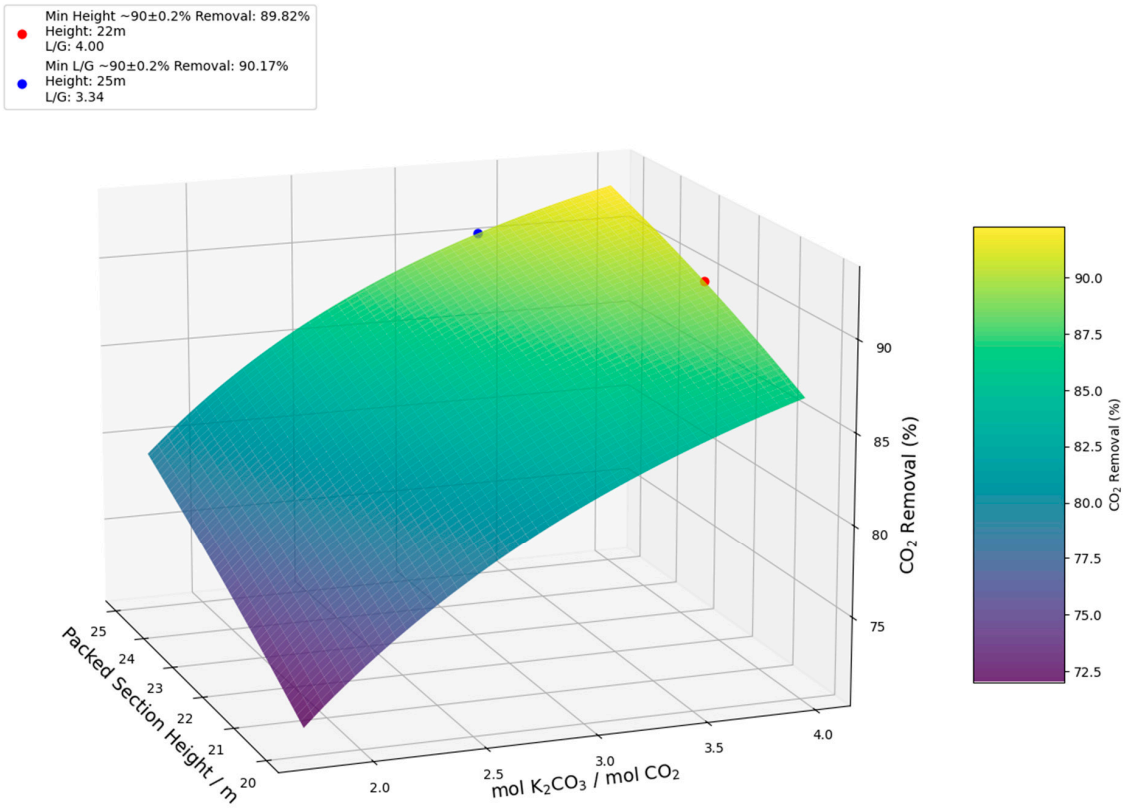


**Figure 9.** Three-dimensional plot of $CO_2$ removal vs. column height and L/G for the cement industry flue gas.

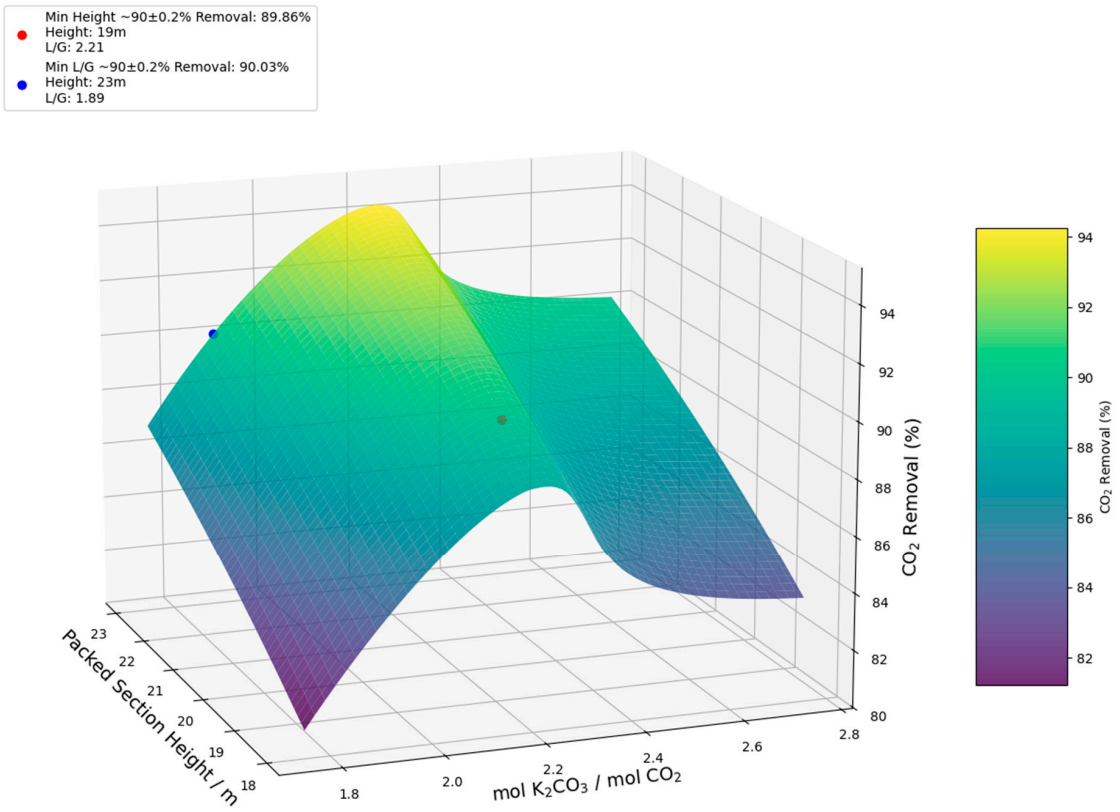


**Figure 10.** Three-dimensional plot of $CO_2$ removal vs. column height and L/G for the biomass combustion flue gas.

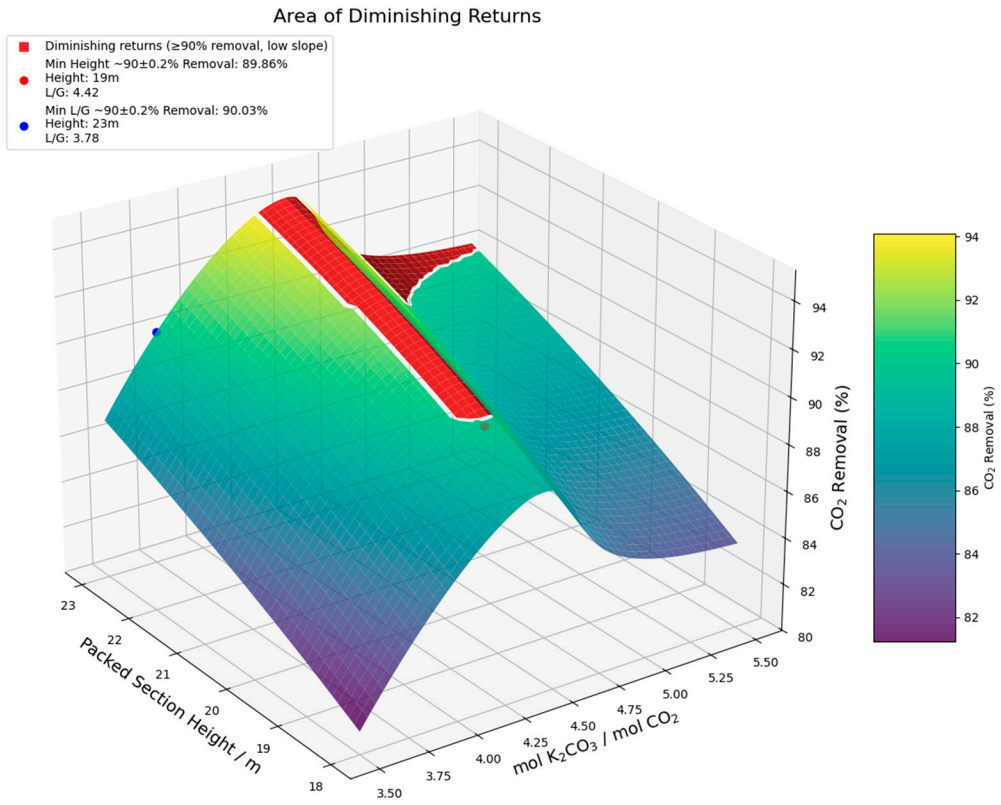


**Figure 11.** Diminishing returns area for biomass combustion scenario.

Figure 9 illustrates two minimum operating points on the surface. The first (red marker) indicates the minimum height required (22 m) for the removal of approximately 90% $CO_2$ at a relatively higher L/G ratio of 4.00. The second (blue marker) indicates the lowest L/G ratio needed (3.34) for the same level of removal efficiency but in a taller column (23 m). These factors decide the chemical consumption versus equipment size tradeoff: increased solvent flow can reduce capital cost in terms of column height, while increased column allows reduced chemical consumption, thus reducing operating costs and energy requirements for solvent recovery.

The response surface shows a small degree of nonlinearity in trend, especially at higher L/G ratios, where the law of diminishing returns to removal efficiency becomes evident. Eventually, additional increase to the L/G ratio no longer returns proportional improvements in performance, and therefore maximum solvent utilization can be identified for minimizing operating costs. Finally, this case exhibits the highest solvent loading requirements, as well as the highest column height for the effective removal of $CO_2$.

Figure 10 presents the two minimum operating points for the biomass combustion case. The first (red marker) corresponds to the minimum height required (19 m) to achieve approximately 90% $CO_2$ removal, at a molar L/G ratio of 2.21. The second (blue marker) corresponds to the minimum L/G ratio (1.89) to achieve the same target, for a column slightly taller (23 m). These points demonstrate again the trade-off between solvent usage and column design, allowing flexibility depending on economic or operational priorities.

As observed before in Figure 7, an interesting behavior of this case is the presence of a peak followed by a drop in $CO_2$ removal efficiency as the L/G ratio increases beyond ~2.25. This local optimum appears due to the optimization of the (L/G—Temperature) parameter set in the process. It indicates that in flue gases with higher water vapor content, energy integration through heat exchanger is essential for solvent, thus energy savings.

For this case, a diminishing-returns region was defined as the subset of the operating space satisfying two conditions: (i) $CO_2$ removal equal to or greater than the design target

of 90%, and (ii) low local sensitivity, identified as gradient magnitudes within the lowest 20% of all computed values. This criterion isolates regions where further increases in height or L/G result in only marginal improvements in removal performance. The identified region is highlighted directly on the three-dimensional removal surface in Figure 11.

Figure 11 shows that the 90% removal target is not achieved at a single, sharply defined operating point but rather across a flat trade-off region where the surface slope is low. Within this region, substantial increases in packed height or L/G yield only minor gains in $CO_2$ removal, indicating diminishing returns.

The two reported "optima"—minimum packed height and minimum L/G—represent limiting design choices on this plateau. While they differ in operational emphasis, both lie within the same low-sensitivity region and, therefore, provide essentially equivalent capture performance. As a result, the optimum is not unique in a practical sense. Instead, final design selection within this region may be guided by secondary considerations such as column footprint, hydraulic constraints, solvent circulation costs, or retrofit limitations, without materially affecting removal efficiency.

Overall, the case indicates the importance of process optimization, as solvent overfeeding will result in deteriorating or even negative returns on capture efficiency. Defining both minimum column height and solvent loading to reach performance goals allows for flexible design and cost trade-off.

Figure 12 illustrates two minimum operating points for anaerobic digestion case. The first (red marker) indicates the minimum height required (18 m) to achieve approximately 90% $CO_2$ removal, at a molar L/G ratio of 1.53. The second (blue marker) corresponds to the minimum L/G ratio (1.41) to achieve the same target, for a taller column (20 m). These points demonstrate again the trade-off between solvent usage and column design, allowing flexibility depending on economic or operational priorities.

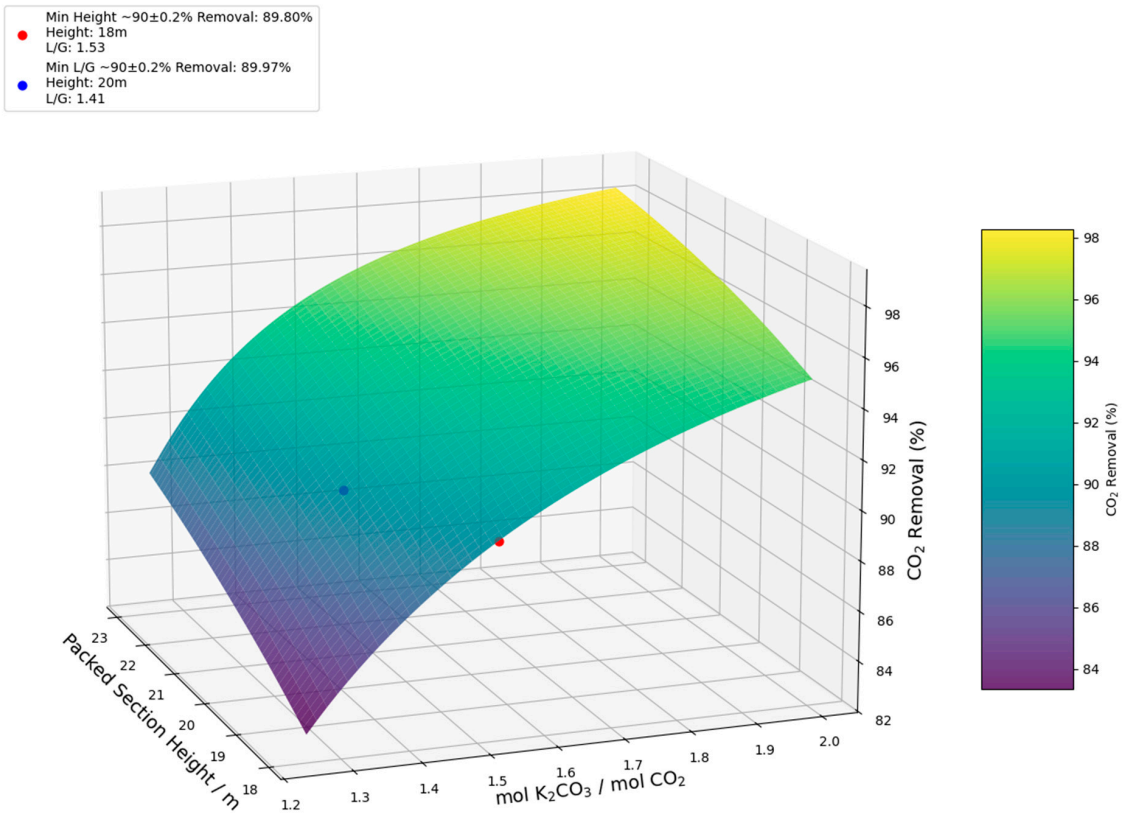


**Figure 12.** Three-dimensional plot of $CO_2$ removal vs. column height and L/G for the anaerobic digestion biogas.

These results demonstrate the lowest L/G values between all the cases, but they are not comparable to the other cases as they derived from a process with a solvent temperature of 45 °C. Energy integration was not feasible in this case, as the produced biogas is usually around 35 °C. Nevertheless, the high $CO_2$ content in biogas enhances the driving force of the chemical absorption, while the presence of bicarbonates in the solvent lowers the reaction's activation energy—improving efficiency at elevated temperatures. These conditions make potassium carbonate-based solvents a technically feasible option for biogas upgrading. The cumulative results for each optimal point are presented in Table 7.

**Table 7.** Minimum operating and design parameters for each scenario.

| Scenario | Cement Industry | | Biomass Combustion | | Anaerobic Digestion | |
|---|---|---|---|---|---|---|
| **Constraint** | **Min. Height** | **Min. L/G** | **Min. Height** | **Min. L/G** | **Min. Height** | **Min. L/G** |
| Column height (m) | 22 | 25 | 19 | 23 | 18 | 20 |
| mol $K_2CO_3$/mol $CO_2$ | 4.00 | 3.34 | 2.21 | 1.89 | 1.53 | 1.41 |
| Solvent/Gas mass ratio | 12.88 | 11.50 | 3.46 | 2.96 | 15.92 | 14.21 |
| $CO_2$ Removal (%) | 89.82 | 90.17 | 89.86 | 90.03 | 89.80 | 89.97 |

Table 7 summarizes the operating and design parameters across the three scenarios. In every scenario the targeted $CO_2$ removal was achieved, indicating that potassium carbonate is a technically viable solvent.

The column height varied between 18 and 25 m for all cases. This implies higher capital expenditures when compared to MEA-based systems which typically operate within 6 to 12 m is similar scenarios [61].

Molar ratios between scenarios range within relatively small limits, as opposed to the L/G mass ratios, where they show great variations in the case of the cement industry and AD flue gases. These cases show significantly higher requirement of solvent mass rate when compared to the biomass combustion scenario, which suggests elevated energy and material demands. The elevated solvent requirement is attributed to the higher $CO_2$ composition in those gases. Even though the higher partial pressure of $CO_2$ increases the driving force of absorption, the kinetic rate remains at a level where large solvent quantities are required.

While the molar ratios required for the potassium carbonate solvent are moderately higher (ranging from 1.41 to 4.00) than those reported for MEA which typically range between 1.00 and 2.00 [62–64], the mass ratios differ significantly. This discrepancy stems from the difference in molecular weights between the two solvents: 138.21 g $mol^{-1}$ for $K_2CO_3$ versus 61.08 g $mol^{-1}$ for MEA and, from the slower reaction kinetics of the carbonate system.

To address regeneration feasibility, a simplified stripper section was appended downstream of the absorber for each case, using the corresponding $CO_2$-rich solvent stream as feed. Table 8 reports preliminary rich $CO_2$ loadings and the associated reboiler duty normalized per tonne of $CO_2$ regenerated. These values are intended as first-pass estimates, because detailed heat integration (e.g., lean–rich exchanger optimization), pressure/temperature optimization, and advanced regeneration configurations were not implemented at this stage. Nevertheless, the results provide an initial basis for comparing the relative regeneration demand among the investigated operating cases and highlight regeneration-energy optimization as a key direction for future work.

**Table 8.** Preliminary stripper performance indicators and estimated regeneration energy.

| Scenario | Cement Industry | | Biomass Combustion | | Anaerobic Digestion | |
|---|---|---|---|---|---|---|
| **Constraint** | **Min. Height** | **Min. L/G** | **Min. Height** | **Min. L/G** | **Min. Height** | **Min. L/G** |
| Column height (m) | 22 | 25 | 19 | 23 | 18 | 20 |
| mol $CO_2$/mol $K_2CO_3$ | 0.275 | 0.261 | 0.223 | 0.284 | 0.354 | 0.372 |
| Specific reboiler duty ($GJ/ton_{CO2}$) | 3.72 | 3.47 | 4.15 | 3.94 | 2.69 | 2.59 |

The calculated lean solvent loadings at the stripper outlet range between 0.223 and 0.372 mol $CO_2$ $mol^{-1}$ $K_2CO_3$, reflecting differences in inlet gas composition, solvent circulation rate, and operating temperature among the three cases.

The estimated specific reboiler duty varies from 2.59 to 4.15 GJ $t^{-1}$ $CO_2$. The anaerobic digestion case exhibits the lowest regeneration energy demand (2.59–2.69 GJ $t^{-1}$ $CO_2$), which is attributed to the higher $CO_2$ partial pressure, resulting in increased cyclic capacity. In contrast, the biomass combustion scenario shows the highest regeneration energy requirement (3.94–4.15 GJ $t^{-1}$ $CO_2$), despite its lower solvent circulation rates, due to the lower $CO_2$ driving force in the absorber and reduced cyclic loading. The cement industry case yields intermediate regeneration energy values (3.47–3.72 GJ $t^{-1}$ $CO_2$), consistent with its moderate $CO_2$ concentration and solvent loading.

### *3.2. Model Validation*

Direct experimental validation of the present model was not conducted within this study; therefore, the developed rate-based Aspen Plus model was validated against published pilot-scale and demonstration-scale data for potassium carbonate $CO_2$ absorption systems. This approach is commonly adopted for absorption modeling studies, particularly when well-documented experimental benchmarks are available in the literature.

#### 3.2.1. Validation Against Pilot-Scale Potassium Carbonate Absorption Studies

Smith et al. [65] investigated $CO_2$ capture using 20–40 wt% potassium carbonate solutions in both laboratory-scale and industrial pilot plants and developed Aspen Plus models to predict absorber performance. Their work demonstrated that rate-based Aspen Plus simulations employing the ELECNRTL thermodynamic model, Onda correlations for mass transfer, and literature-based reaction kinetics could predict $CO_2$ removal efficiencies, solvent loadings, and temperature profiles within ±5% of experimental measurements.

They also reported stable operation and accurate model predictions for $CO_2$ removal efficiencies ranging from approximately 80–95%, depending on solvent concentration, liquid-to-gas (L/G) ratio, and column height. These removal levels are consistent with the 90% $CO_2$ capture target adopted in the present study. Furthermore, the solvent concentrations (20 wt% $K_2CO_3$) and operating temperature ranges employed in the present model fall well within the experimentally validated ranges reported in their pilot-scale investigations.

The absorber packing heights reported were on the order of 3–6 m at pilot scale, which, when scaled to industrial gas flow rates and comparable L/G ratios, translate to absorber heights in the range of 15–30 m. This range is in good agreement with the 18–25 m column heights predicted by the present model, supporting the physical realism of the simulation results.

#### 3.2.2. Validation Against Demonstration-Scale Potassium Carbonate Processes

Further validation is obtained by comparison with the demonstration-scale potassium carbonate capture process reported, where a concentrated $K_2CO_3$ system was successfully operated at up to 1 tonne $CO_2$ per day using flue gas from a coal-fired power station. In

that work, Aspen Plus simulations were used to predict absorber performance, solvent circulation rates, and $CO_2$ removal efficiencies, and were shown to be in close agreement with measured plant data [66].

The demonstration plant achieved $CO_2$ removal efficiencies approaching 90% at solvent loadings and L/G ratios comparable to those identified as optimal in the present study. The authors highlighted that potassium carbonate systems require larger absorber heights and higher solvent circulation rates than MEA systems, due to slower reaction kinetics—an observation that is directly reflected in the current modeling results. The predicted solvent-to-gas mass ratios and column heights in this work are therefore consistent with validated industrial-scale potassium carbonate capture systems.

#### 3.2.3. Consistency with Independent Aspen Plus Simulation Studies

Additional validation is provided by comparison with independent Aspen Plus simulation studies of potassium carbonate-based $CO_2$ capture processes. Chuenphan et al. [67] performed a techno-economic and sensitivity analysis of $CO_2$ capture using $K_2CO_3$ solutions and demonstrated that Aspen Plus simulations could reliably predict $CO_2$ removal efficiencies between 85 and 90%, solvent circulation requirements, and energy consumption trends when benchmarked against experimental data.

Their results confirmed that L/G ratio and inlet $CO_2$ concentration are the dominant parameters controlling removal efficiency—findings that are fully consistent with the sensitivity trends observed in Figures 4–9 of the present study. Moreover, the solvent loadings reported by Chuenphan et al. (typically 1.5–4.0 mol $K_2CO_3$ per mol $CO_2$) align closely with the optimal ranges predicted here (1.41–4.00 mol $K_2CO_3$/mol $CO_2$), further supporting the validity of the model outputs.

#### 3.2.4. Overall Validation Assessment

Taken together, comparison with pilot-scale experiments, demonstration-scale operation, and independent Aspen Plus simulation studies confirms that the present rate-based model reliably captures the dominant physical, chemical, and mass-transfer phenomena governing $CO_2$ absorption in potassium carbonate systems. The predicted $CO_2$ removal efficiencies, solvent loadings, and absorber height requirements fall squarely within ranges that have been experimentally observed and previously validated in the literature.

## 4. Discussion

The present study evaluated the technical feasibility of potassium carbonate–based $CO_2$ capture across three representative industrial gas streams, with particular emphasis on absorber design requirements, solvent utilization, and preliminary regeneration energy demand. By combining absorber sensitivity analysis with simplified stripper simulations, the results allow a first-order comparison of capture performance and regeneration intensity across cases with markedly different $CO_2$ concentrations and thermal characteristics.

For the cement industry flue gas, relatively high solvent circulation rates and molar $K_2CO_3/CO_2$ ratios were required to achieve the target $CO_2$ removal efficiency. Optimal operating points corresponded to molar ratios between 3.34 and 4.00, reflecting the high inlet $CO_2$ concentration and the slower intrinsic kinetics of the carbonate system. These conditions translated into intermediate regeneration energy demands, with specific reboiler duties ranging from 3.47 to 3.72 GJ $t^{-1}$ $CO_2$. While these values remain below or comparable to typical MEA-based systems, they indicate that solvent regeneration constitutes a significant energetic contribution for cement applications, particularly when high solvent loadings are required. The results suggest that cement flue gas capture with potassium

carbonate is technically feasible, but optimization of cyclic loading and solvent circulation is essential to avoid excessive regeneration duties.

The biomass combustion scenario exhibited the most favorable overall behavior among the investigated cases. Due to the lower $CO_2$ concentration in the flue gas and the high water vapor content, lower molar solvent ratios (1.89–2.21 mol $K_2CO_3$ per mol $CO_2$) were sufficient to reach 90% removal. Despite this, the biomass case showed the highest specific regeneration energy (3.94–4.15 GJ $t^{-1}$ $CO_2$). This apparent contradiction is explained by the reduced cyclic loading of the solvent under low $CO_2$ partial pressure conditions, which limits the amount of $CO_2$ released per unit of circulating solvent.

A distinctive feature of the biomass case was the presence of a clear diminishing-returns region, where increases in L/G ratio or column height produced marginal or even negative gains in $CO_2$ removal efficiency. This behavior arises from the interaction between mass transfer and thermal effects: excessive solvent flow reduces interfacial temperature due to heat imbalance between the cold liquid and the hot, humid gas stream, thereby decreasing solvent capacity. From a process design perspective, this highlights the importance of avoiding solvent overfeeding and operating within a narrow optimal window. Nevertheless, the ability to exploit sensible heat from the flue gas renders biomass combustion particularly attractive for potassium carbonate systems when appropriate energy integration is applied.

The anaerobic digestion (AD) case showed the lowest specific regeneration energy demand, with reboiler duties between 2.59 and 2.69 GJ $t^{-1}$ $CO_2$. This reduction is primarily attributed to the high $CO_2$ partial pressure in biogas and the elevated solvent operating temperature (45 °C), both of which enhance cyclic loading and facilitate solvent regeneration. However, this apparent energetic advantage must be interpreted with caution. The AD scenario required the highest solvent circulation rates and solvent-to-gas mass ratios among all cases, driven by the very high inlet $CO_2$ concentration. As a result, while the normalized regeneration energy is low, the absolute energy consumption and solvent handling requirements are substantial. This indicates a potential inefficiency at the system level, where low specific heat duty does not necessarily translate into overall process optimality.

Across all scenarios, the predicted regeneration energies and solvent loadings fall within ranges reported in previous simulation and pilot-scale studies of potassium carbonate systems. Reported reboiler duties in the literature [67] typically range from approximately 2.0 to 4.5 GJ $t^{-1}$ $CO_2$, depending on solvent concentration, lean loading, and operating conditions. The values obtained in this work are, therefore, consistent with established trends and further support the validity of the modeling approach. The results reinforce the general observation that potassium carbonate systems can achieve regeneration energy requirements lower than conventional MEA systems, albeit at the expense of higher solvent circulation rates and larger absorber dimensions.

Overall, the comparative analysis demonstrates that potassium carbonate is best suited to applications where moderate $CO_2$ concentrations and favorable thermal integration opportunities exist, while high-$CO_2$ streams may require careful balancing between regeneration efficiency and solvent throughput.

*Limitations and Directions for Future Work*

Despite the insights provided by this study, several limitations should be acknowledged. First, the reaction kinetics employed in the rate-based model were derived entirely from literature sources, and no experimental data were available for regression or recalibration under the specific operating conditions examined. While the selected kinetics are well established, experimental validation at pilot scale would improve confidence in predicted mass-transfer and loading behavior.

Second, the regeneration energy estimates presented here are preliminary. The stripper was modeled in a simplified configuration, without detailed optimization of operating pressure, or advanced regeneration schemes such as multi-pressure stripping or vapor recompression. As a result, the reported reboiler duties should be interpreted as indicative rather than optimal values.

Third, a full techno-economic assessment was outside the scope of this work. Capital costs associated with larger absorber columns, increased solvent circulation, and heat-exchange equipment were not quantified, nor were operating costs beyond reboiler energy considered. Such analysis is essential for assessing the overall feasibility of potassium carbonate systems relative to amine-based technologies.

Future work should, therefore, focus on

1. Experimental validation of absorption and regeneration performance;
2. Detailed energy integration and optimization of the regeneration section;
3. Comprehensive techno-economic and exergy analyses;
4. Systematic investigation of alternative solvent formulations, including different $K_2CO_3$ concentrations and carbonate-to-bicarbonate (CTB) conversion levels, to evaluate their impact on cyclic capacity and reboiler duty.

Addressing these aspects will be critical for advancing potassium carbonate systems from technical feasibility toward industrial implementation.

## 5. Conclusions

This study investigated the application of aqueous potassium carbonate solutions for post-combustion and biogas $CO_2$ capture through detailed rate-based process simulations. Three representative industrial gas streams—cement production, biomass combustion, and anaerobic digestion—were examined under consistent throughput conditions to assess absorber design requirements, solvent utilization, and preliminary regeneration energy demand.

The simulation results confirm that potassium carbonate systems can technically achieve high $CO_2$ removal efficiencies, approaching 90% across all investigated cases, when appropriate combinations of column height and solvent circulation rate are applied. Achieving this level of performance required packed column heights between 18 and 25 m and molar $K_2CO_3/CO_2$ ratios ranging from approximately 1.4 to 4.0, depending on the inlet gas composition. These requirements are higher than those typically reported for fast-reacting amine solvents and reflect the lower intrinsic reaction kinetics of carbonate-based systems.

The comparative analysis revealed distinct behavior among the three cases. Biomass combustion flue gas showed the most balanced absorber performance, requiring relatively moderate solvent loadings while benefiting from favorable thermal conditions and opportunities for heat integration. However, the presence of a diminishing-returns region with increasing solvent circulation highlights that process optimization is essential, as solvent overfeeding may lead to reduced absorption efficiency and unnecessary energy penalties.

In the anaerobic digestion scenario, the high $CO_2$ partial pressure resulted in enhanced cyclic loading and the lowest specific regeneration energy demand among the cases studied. Nevertheless, this advantage was accompanied by high solvent circulation rates and solvent-to-gas mass ratios, suggesting that low normalized reboiler duty does not necessarily imply overall process efficiency when evaluated at the system level. The cement industry case exhibited intermediate behavior, combining relatively high solvent loading requirements with moderate regeneration energy demand, consistent with its elevated $CO_2$ concentration.

Preliminary stripper simulations indicated regeneration energy requirements between 2.6 and 4.2 GJ $t^{-1}$ $CO_2$ across all scenarios. These values are in line with ranges reported in

the literature for potassium carbonate systems and generally lower than those associated with conventional MEA-based processes. However, the regeneration section was not optimized in detail, and the reported values should be interpreted as indicative estimates rather than optimized benchmarks.

Overall, the results suggest that potassium carbonate can be considered a technically feasible solvent for $CO_2$ capture in selected industrial applications, particularly where solvent stability, low volatility, and reduced degradation are important considerations. At the same time, the higher solvent circulation rates and larger absorber dimensions required relative to amine-based systems represent important trade-offs that must be accounted for in the process design.

In conclusion, potassium carbonate does not constitute a universal substitute for amine solvents, but it represents a credible alternative for specific applications where its advantages can be effectively leveraged. Further experimental validation, detailed regeneration optimization, and comprehensive techno-economic analysis are required before definitive conclusions regarding its industrial competitiveness can be drawn.

**Author Contributions:** Conceptualization, G.P. and D.M.; methodology, G.P. and S.M.; software, G.P.; validation, G.P., S.M. and E.M.B.; formal analysis, G.P.; investigation, G.P., S.M., E.M.B. and D.M.; resources, G.P. and E.M.B.; data curation, G.P., S.M. and E.M.B.; writing—original draft preparation, G.P.; writing—review and editing, S.M., E.M.B. and D.M.; visualization, G.P. and S.M.; supervision, D.M.; project administration, D.M.; funding acquisition, D.M. All authors have read and agreed to the published version of the manuscript.

**Funding:** This research was funded by the European Union's Horizon Europe research and innovation programme under grant agreement No. 101084405 (CRONUS).

**Data Availability Statement:** The original contributions presented in this study are included in the article. Further inquiries can be directed to the corresponding authors.

**Conflicts of Interest:** The authors declare no conflict of interest.

## Abbreviations

The following abbreviations are used in this manuscript:

| | |
|---|---|
| AD | Anaerobic Digestion |
| CCS | Carbon Capture and Storage |
| CCU | Carbon Capture and Utilization |
| CCUS | Carbon Capture, Utilization and Storage |
| CTB | Carbonate-to-Bicarbonate Conversion |
| DMEA | Dimethylethanolamine |
| ELECNRTL | Electrolyte Non-Random Two-Liquid Model |
| GJ | Gigajoule |
| GML | Global Monitoring Laboratory |
| IPCC | Intergovernmental Panel on Climate Change |
| L/G | Liquid-to-Gas Ratio |
| MEA | Monoethanolamine |
| PZ | Piperazine |
| RK | Redlich–Kwong Equation of State |
| TGME | Triethylene glycol monomethyl ether |
| UNFCCC | United Nations Framework Convention on Climate Change |
| VLE | Vapor–Liquid Equilibrium |

## References


1. Gulev, S.K.; Thorne, P.W.; Ahn, J.; Dentener, F.J.; Domingues, C.M.; Gerland, S.; Gong, D.; Kaufman, D.S.; Nnamchi, H.C.; Quaas, J.; et al. Changing state of the climate system. In *Climate Change 2021: The Physical Science Basis. Contribution of Working Group I to the Sixth Assessment Report of the Intergovernmental Panel on Climate Change*; Masson-Delmotte, V., Zhai, P., Pirani, A., Connors, S.L., Péan, C., Berger, S., Caud, N., Chen, Y., Goldfarb, L., Gomis, M.I., et al., Eds.; Cambridge University Press: Cambridge, UK, 2021; pp. 287–422, ISBN 978-1-009-15789-6. Available online: https://centaur.reading.ac.uk/101849/ (accessed on 11 April 2025).
2. Lan, X.; Tans, P.; Thoning, K. *NOAA Global Monitoring Laboratory Trends in Globally-Averaged $CO_2$ Determined from NOAA Global Monitoring Laboratory Measurements*; Global Monitoring Laboratory: Boulder, CO, USA, 2025. [CrossRef]
3. Friedlingstein, P.; O'Sullivan, M.; Jones, M.W.; Andrew, R.M.; Hauck, J.; Landschützer, P.; Le Quéré, C.; Li, H.; Luijkx, I.T.; Olsen, A.; et al. Global Carbon Budget 2024. *Earth Syst. Sci. Data* **2025**, *17*, 965–1039. [CrossRef]
4. Andrew, R.M. Global $CO_2$ emissions from cement production. *Earth Syst. Sci. Data* **2018**, *10*, 195–217. [CrossRef]
5. Qu, G.; Shi, Y.; Yang, Y.; Wu, W.; Zhou, Z. Methods, Progress and Challenges in Global Monitoring of Carbon Emissions from Biomass Combustion. *Atmosphere* **2024**, *15*, 1247. [CrossRef]
6. UNFCCC. The Paris Agreement. In Proceedings of the UN Climate Change Conference (COP21), Paris, France, 12 December 2015.
7. IPCC. Climate change 2022: Mitigation of climate change. In *Contribution of Working Group III to the Sixth Assessment Report*; IPCC: Geneva, Switzerland, 2022. Available online: https://www.ipcc.ch/report/ar6/wg3/ (accessed on 11 April 2025).
8. Hanson, E.; Nwakile, C.; Hammed, V.O. Carbon capture, utilization, and storage (CCUS) technologies: Evaluating the effectiveness of advanced CCUS solutions for reducing $CO_2$ emissions. *Results Surf. Interfaces* **2025**, *18*, 100381. [CrossRef]
9. Do, C.V.T.; Nguyen, N.T.T.; Tran, T.D.; Pham, M.H.T.; Pham, T.Y.T. Capability of carbon fixation in bicarbonate-based and carbon dioxide-based systems by *Scenedesmus acuminatus* TH04. *Biochem. Eng. J.* **2021**, *166*, 107858. [CrossRef]
10. Yang, Y.; Tang, S.; Chen, J.P. Carbon capture and utilization by algae with high concentration $CO_2$ or bicarbonate as carbon source. *Sci. Total Environ.* **2024**, *918*, 170325. [CrossRef] [PubMed]
11. Duma, Z.G.; Dyosiba, X.; Moma, J.; Langmi, H.W.; Louis, B.; Parkhomenko, K.; Musyoka, N.M. Thermocatalytic Hydrogenation of $CO_2$ to Methanol Using Cu-ZnO Bimetallic Catalysts Supported on Metal–Organic Frameworks. *Catalysts* **2022**, *12*, 401. [CrossRef]
12. Chen, C.; Zhu, X.; Wen, X.; Zhou, Y.; Zhou, L.; Li, H.; Tao, L.; Li, Q.; Du, S.; Liu, T.; et al. Coupling $N_2$ and $CO_2$ in $H_2O$ to synthesize urea under ambient conditions. *Nat. Chem.* **2020**, *12*, 717–724. [CrossRef]
13. Ye, J.; Fang, J.; Sun, Y.; Shi, X.; Chen, G.; Ma, T.; Zhi, X. $CO_2$ mineralization of cement-based materials by accelerated $CO_2$ mineralization and its mineralization degree: A review. *Constr. Build. Mater.* **2024**, *444*, 137712. [CrossRef]
14. Li, Y.; Guan, B.; Guo, J.; Chen, Y.; Ma, Z.; Zhuang, Z.; Zhu, C.; Dang, H.; Chen, L.; Shu, K.; et al. Renewable synthetic fuels: Research progress and development trends. *J. Clean. Prod.* **2024**, *450*, 141849. [CrossRef]
15. Raganati, F.; Ammendola, P. CO2 Post-combustion Capture: A Critical Review of Current Technologies and Future Directions. *Energy Fuels* **2024**, *38*, 13858–13905. [CrossRef]
16. Kothandaraman, A. Carbon Dioxide Capture by Chemical Absorption: A Solvent Comparison Study. Ph.D. Thesis, Massachusetts Institute of Technology, Cambridge, MA, USA, 2010.
17. Kohl, A.L.; Nielsen, R. *Gas Purification*; Elsevier: Amsterdam, The Netherlands, 1997; ISBN 978-0-08-050720-0.
18. Tobiesen, A.; Mejdell, T.; Svendsen, H.F. A Comparative Study of Experimental and Modeling Performance Results from the CASTOR Esbjerg Pilot Plant. 2006. Available online: https://www.osti.gov/etdeweb/biblio/20847672 (accessed on 11 April 2025).
19. Goff, G.S.; Rochelle, G.T. Oxidation Inhibitors for Copper and Iron Catalyzed Degradation of Monoethanolamine in $CO_2$ Capture Processes. *Ind. Eng. Chem. Res.* **2006**, *45*, 2513–2521. [CrossRef]
20. McCann, N.; Phan, D.; Wang, X.; Conway, W.; Burns, R.; Attalla, M.; Puxty, G.; Maeder, M. Kinetics and Mechanism of Carbamate Formation from $CO_2$(aq), Carbonate Species, and Monoethanolamine in Aqueous Solution. *J. Phys. Chem. A* **2009**, *113*, 5022–5029. [CrossRef]
21. Sexton, A.; Rochelle, G.T. Oxidation products of amines in $CO_2$ capture. In Proceedings of the Eighth International Conference on Greenhouse Gas Control Technologies, Trondheim, Norway, 19–22 June 2006.
22. Stergioudi, F.; Baxevani, A.; Florou, C.; Michailidis, N.; Nessi, E.; Papadopoulos, A.I.; Seferlis, P. Corrosion Behavior of Stainless Steels in $CO_2$ Absorption Process Using Aqueous Solution of Monoethanolamine (MEA). *Corros. Mater. Degrad.* **2022**, *3*, 422–438. [CrossRef]
23. Reynolds, A.J.; Verheyen, T.V.; Adeloju, S.B.; Meuleman, E.; Feron, P. Towards Commercial Scale Postcombustion Capture of $CO_2$ with Monoethanolamine Solvent: Key Considerations for Solvent Management and Environmental Impacts. *Environ. Sci. Technol.* **2012**, *46*, 3643–3654. [CrossRef] [PubMed]
24. Dubey, A.; Arora, A. Advancements in carbon capture technologies: A review. *J. Clean. Prod.* **2022**, *373*, 133932. [CrossRef]
25. Vega, F.; Sanna, A.; Navarrete, B.; Maroto-Valer, M.M.; Cortés, V.J. Degradation of amine-based solvents in $CO_2$ capture process by chemical absorption. *Greenh. Gases Sci. Technol.* **2014**, *4*, 707–733. [CrossRef]

26. Xu, B.; Gao, X.; Gao, G.; Jiang, W.; Li, X.; Luo, C.; Wu, F.; Zhang, L. A low viscosity and energy saving phase change absorbent of DMEA/MAE/$H_2O$/TGME for post-combustion $CO_2$ capture. *Chem. Eng. Sci.* **2025**, *304*, 121058. [CrossRef]
27. Borhani, T.N.G.; Azarpour, A.; Akbari, V.; Wan Alwi, S.R.; Manan, Z.A. $CO_2$ capture with potassium carbonate solutions: A state-of-the-art review. *Int. J. Greenh. Gas Control* **2015**, *41*, 142–162. [CrossRef]
28. Zhang, P.; Sun, Q.; Dong, Y.; Lian, S. Effects of different bicarbonate on spirulina in $CO_2$ absorption and microalgae conversion hybrid system. *Front. Bioeng. Biotechnol.* **2023**, *10*, 1119111. [CrossRef]
29. Yeh, K.-L.; Chang, J.-S.; Chen, W. Effect of light supply and carbon source on cell growth and cellular composition of a newly isolated microalga Chlorella vulgaris ESP-31. *Eng. Life Sci.* **2010**, *10*, 201–208. [CrossRef]
30. Abinandan, S.; Shanthakumar, S. Evaluation of photosynthetic efficacy and $CO_2$ removal of microalgae grown in an enriched bicarbonate medium. *3 Biotech* **2016**, *6*, 9. [CrossRef]
31. Budzianowski, W.M. (Ed.) *Energy Efficient Solvents for $CO_2$ Capture by Gas-Liquid Absorption: Compounds, Blends and Advanced Solvent Systems*; Green Energy and Technology; Springer International Publishing: Cham, Switzerland, 2017. [CrossRef]
32. Fan, Z.; Liu, K.; Qi, G.; Frimpong, R.; Nikolic, H.; Liu, K. Aspen modeling for MEA–$CO_2$ loop: Dynamic gridding for accurate column profile. *Int. J. Greenh. Gas Control* **2015**, *37*, 318–324. [CrossRef]
33. Garcia, M.; Knuutila, H.K.; Gu, S. ASPEN PLUS simulation model for $CO_2$ removal with MEA: Validation of desorption model with experimental data. *J. Environ. Chem. Eng.* **2017**, *5*, 4693–4701. [CrossRef]
34. Kopac, T.; Demirel, Y. Optimizing $CO_2$ capture from biogas: A comparative study of amine-based solvents through Aspen Plus simulations. *Biomass Convers. Biorefinery* **2025**, *15*, 21327–21347. [CrossRef]
35. Majnoon, A.; Hajinezhad, A.; Moosavian, S.F. Simulation model of carbon capture with MEA and the effect of temperature and duty on efficiency. *Future Energy* **2024**, *3*, 37–47. [CrossRef]
36. Wang, N.; Wang, D.; Krook-Riekkola, A.; Ji, X. MEA-based $CO_2$ capture: A study focuses on MEA concentrations and process parameters. *Front. Energy Res.* **2023**, *11*, 1230743. [CrossRef]
37. Yang, Y.; Du, T.; Li, Y.; Yue, Q.; Wang, H.; Liu, L.; Che, S.; Wang, Y. Techno-economic assessment and exergy analysis of iron and steel plant coupled MEA-$CO_2$ capture process. *J. Clean. Prod.* **2023**, *416*, 137976. [CrossRef]
38. Cabello, A.; Mendiara, T.; Abad, A.; Adánez, J. Techno-economic analysis of a chemical looping combustion process for biogas generated from livestock farming and agro-industrial waste. *Energy Convers. Manag.* **2022**, *267*, 115865. [CrossRef]
39. European Biogas Association. *EBA Statistical Report 2024*; European Biogas Association: Etterbeek, Belgium, 2024.
40. Pinsent, B.R.W.; Pearson, L.; Roughton, F.J.W. The kinetics of combination of carbon dioxide with hydroxide ions. *Trans. Faraday Soc.* **1956**, *52*, 1512. [CrossRef]
41. Pohorecki, R.; Moniuk, W. Kinetics of reaction between carbon dioxide and hydroxyl ions in aqueous electrolyte solutions. *Chem. Eng. Sci.* **1988**, *43*, 1677–1684. [CrossRef]
42. Chen, P.-C. Absorption of Carbon Dioxide in a Bubble-Column Scrubber. In *Greenhouse Gases—Capturing, Utilization and Reduction*; Liu, G., Ed.; InTech: London, UK, 2012. [CrossRef]
43. Sirs, J.A. Electrometric stopped flow measurements of rapid reactions in solution. Part 2.—Glass electrode pH measurements. *Trans. Faraday Soc.* **1958**, *54*, 207–212. [CrossRef]
44. Pinsent, B.R.W.; Roughton, F.J.W. The kinetics of combination of carbon dioxide with water and hydroxide ions. *Trans. Faraday Soc.* **1951**, *47*, 263. [CrossRef]
45. Himmelblau, D.M.; Babb, A.L. Kinetic studies of carbonation reactions using radioactive tracers. *AIChE J.* **1958**, *4*, 143–152. [CrossRef]
46. Hikita, H.; Asai, S.; Takatsuka, T. Absorption of carbon dioxide into aqueous sodium hydroxide and sodium carbonate-bicarbonate solutions. *Chem. Eng. J.* **1976**, *11*, 131–141. [CrossRef]
47. Kucka, L.; Kenig, E.Y.; Górak, A. Kinetics of the Gas−Liquid Reaction between Carbon Dioxide and Hydroxide Ions. *Ind. Eng. Chem. Res.* **2002**, *41*, 5952–5957. [CrossRef]
48. Ye, X.; Lu, Y. Kinetics of $CO_2$ absorption into uncatalyzed potassium carbonate–bicarbonate solutions: Effects of $CO_2$ loading and ionic strength in the solutions. *Chem. Eng. Sci.* **2014**, *116*, 657–667. [CrossRef]
49. Vázquez, G.; Chenlo, F.; Pereira, G. Enhancement of the Absorption of $CO_2$ in Alkaline Buffers by Organic Solutes: Relation with Degree of Dissociation and Molecular OH Density. *Ind. Eng. Chem. Res.* **1997**, *36*, 2353–2358. [CrossRef]
50. Voldsund, M.; Gardarsdottir, S.O.; De Lena, E.; Pérez-Calvo, J.-F.; Jamali, A.; Berstad, D.; Fu, C.; Romano, M.; Roussanaly, S.; Anantharaman, R.; et al. Comparison of Technologies for $CO_2$ Capture from Cement Production—Part 1: Technical Evaluation. *Energies* **2019**, *12*, 559. [CrossRef]
51. Angelovič, M.; Findura, P.; Jobbágy, J.; Fiantoková, S.; Križan, M. The measurement of gas emissions status during the combustion of wood chips. *Savrem. Poljopr. Teh.* **2014**, *40*, 221–228. [CrossRef]
52. Piadeh, F.; Offie, I.; Behzadian, K.; Rizzuto, J.P.; Bywater, A.; Córdoba-Pachón, J.-R.; Walker, M. A critical review for the impact of anaerobic digestion on the sustainable development goals. *J. Environ. Manag.* **2024**, *349*, 119458. [CrossRef]

53. Barla, R.J.; Raghuvanshi, S.; Gupta, S. Process integration for the biodiesel production from biomitigation of flue gases. In *Waste and Biodiesel*; Elsevier: Amsterdam, The Netherlands, 2022; pp. 191–215. [CrossRef]
54. Kosowska-Golachowska, M.; Luckos, A.; Czakiert, T. Composition of Flue Gases during Oxy-Combustion of Energy Crops in a Circulating Fluidized Bed. *Energies* **2022**, *15*, 6889. [CrossRef]
55. Vega, F.; Cano, M.; Gallego, L.M.; Camino, S.; Camino, J.A.; Navarrete, B. Evaluation of MEA 5 M performance at different $CO_2$ concentrations of flue gas tested at a $CO_2$ capture lab-scale plant. *Energy Procedia* **2017**, *114*, 6222–6228. [CrossRef]
56. Schakel, W.; Hung, C.R.; Tokheim, L.-A.; Strømman, A.H.; Worrell, E.; Ramírez, A. Impact of fuel selection on the environmental performance of post-combustion calcium looping applied to a cement plant. *Appl. Energy* **2018**, *210*, 75–87. [CrossRef]
57. Ryckebosch, E.; Drouillon, M.; Vervaeren, H. Techniques for transformation of biogas to biomethane. *Biomass Bioenergy* **2011**, *35*, 1633–1645. [CrossRef]
58. Atnoorkar, S.; Ghosh, T.; Cooney, G.; Carpenter, A.; Benitez, J. Generating Emissions Inventory for Carbon Capture and Storage Analysis for Carbon-Intensive Industrial Sectors. 2023. Available online: https://research-hub.nrel.gov/en/publications/generating-emissions-inventory-for-carbon-capture-and-storage-ana/ (accessed on 15 December 2025).
59. Onda, K.; Takeuchi, H.; Okumoto, Y. Mass Transfer Coefficients Between Gas and Liquid Phases in Packed Columns. *J. Chem. Eng. Jpn.* **1968**, *1*, 56–62. [CrossRef]
60. Stichlmair, J.; Bravo, J.L.; Fair, J.R. General model for prediction of pressure drop and capacity of countercurrent gas/liquid packed columns. *Gas Sep. Purif.* **1989**, *3*, 19–28. [CrossRef]
61. Chu, F.; Yang, L.; Du, X.; Yang, Y. $CO_2$ capture using MEA (monoethanolamine) aqueous solution in coal-fired power plants: Modeling and optimization of the absorbing columns. *Energy* **2016**, *109*, 495–505. [CrossRef]
62. Harun, N.; Nittaya, T.; Douglas, P.L.; Croiset, E.; Ricardez-Sandoval, L.A. Dynamic simulation of MEA absorption process for CO2 capture from power plants. *Int. J. Greenh. Gas Control* **2012**, *10*, 295–309. [CrossRef]
63. Khaled, F.; Hamad, E.; Traver, M.; Kalamaras, C. Amine-based $CO_2$ capture on-board of marine ships: A comparison between MEA and MDEA/PZ aqueous solvents. *Int. J. Greenh. Gas Control* **2024**, *135*, 104168. [CrossRef]
64. Schäffer, A.; Brechtel, K.; Scheffknecht, G. Comparative study on differently concentrated aqueous solutions of MEA and TETA for $CO_2$ capture from flue gases. *Fuel* **2012**, *101*, 148–153. [CrossRef]
65. Smith, K.H.; Anderson, C.J.; Tao, W.; Endo, K.; Mumford, K.A.; Kentish, S.E.; Qader, A.; Hooper, B.; Stevens, G.W. Pre-combustion capture of $CO_2$—Results from solvent absorption pilot plant trials using 30 wt% potassium carbonate and boric acid promoted potassium carbonate solvent. *Int. J. Greenh. Gas Control* **2012**, *10*, 64–73. [CrossRef]
66. Smith, K.; Xiao, G.; Mumford, K.; Gouw, J.; Indrawan, I.; Thanumurthy, N.; Quyn, D.; Cuthbertson, R.; Rayer, A.; Nicholas, N.; et al. Demonstration of a Concentrated Potassium Carbonate Process for $CO_2$ Capture. *Energy Fuels* **2014**, *28*, 299–306. [CrossRef]
67. Chuenphan, T.; Yurata, T.; Sema, T.; Chalermsinsuwan, B. Techno-economic sensitivity analysis for optimization of carbon dioxide capture process by potassium carbonate solution. *Energy* **2022**, *254*, 124290. [CrossRef]